-RESEARCH PAPER-

International Journal of Mining and Geo-Engineering

IJMGE

IJMGE 56-2 (2022) 139-150

DOI: 10.22059/IJMGE.2021.283899.594819

Geometry determination of galleries and pillars in Chehel Koureh copper mine, Iran

Masoud Cheraghi Seifabad [a, *], Yousef Mirzadeh Koohshahi [a], Ali Bameri [a]

[a] *Department of Mining Engineering, Isfahan University of Technology, Isfahan, Iran*

Article History:

Received: 20 June. 2019.
Revised: 16 June. 2021.
Accepted: 17 June. 2021.

ABSTRACT

Chehel Koureh mine project is located 110 km NW of Zahedan in the southeast of Iran. Due to the great depth of ore deposits, the underground exploitation method was chosen. In this research, the geomechanical parameters were obtained using in situ tests and empirical formulas. The non-pillar continuous mining method (NPCM) was selected as the most appropriate method considering the shape of the ore body and rock mass strength conditions. As the rock mass is fractured and has semi-continuum characteristics, the stability analysis of the shape dimensions was carried out using FLAC 3D software. In the proposed method, a cylindrical pillar with a height of 3.8 meters was located above the stope. For the safety of the drilling machine room and stope roof, height accuracy was required. Five different pillar diameters (i.e., 3, 3.2, 3.4, 3.6, and 3.8 m) were analyzed by considering the critical height and plastic zone created around the pillar. For these five diameters, only the pillar with a diameter of 3 meters had a supercritical height. It was observed that for the pillar with a diameter of 3.8 m, no plastic zone was created and the safety factor for this pillar was obtained 1.11. Due to the restrictions for the application of the proposed mining method i.e. NPCM in Iran, the Miami method was considered as the alternative mining method applicable to the Chehel Koureh copper deposit. Then, the suitable dimensions for stope and pillar were determined by the same software. In the Miami method, there were three spans and two pillars at each stope before the recovery of pillars could be undertaken. The pillars with three widths of, i.e., 5, 6, and 8 meters were studied for the stability analysis. The results demonstrated that a plastic zone was not created only around the pillar with a width of 8 meters, and the safety factor for this pillar was obtained to be 1.56.

Keywords: *Chehel Koureh mine, Non-pillar continuous mining method (NPCM), Miami method, Safety factor.*

1 Introduction

In underground mining, one of the most important issues is always the design of pillars. Issues such as pillars strength estimation, pillars size, and stress focus in pillars are used to calculate the load on the pillars in different modes [1]. The design of pillars is very important in optimizing mining operations, and to achieve a safe and economical design, the number of loads on the pillar and how to distribute them along with the exact behaviour of the pillar and the surrounding environment must be studied [2]. With strain gauges, load cells, and extensometer the behaviour of the pillars can be examined for numerical modelling. These results are used to design mines where pillars break locally due to load-bearing capacity [3]. Mechanical behaviour in deep galleries has been investigated by considering the effect of Excavation Disturbed Zone (EDZ) using the three-dimensional numerical solution method in two modes; with and without the support system, which can result in reducing the plastic zone in the presence of the support system in gallery ends. Using the rock samples in parallel and series next to each other, the fracture process of rock slabs was investigated. The results of the numerical solution show that not only the stiffness but also the uniaxial compressive strength of the rock play an important role in the stability of the rock pillar. For deep underground structures, the strength of rock masses and induced stresses affect the design of the excavated space and the number of initial stresses. Thus, it is necessary to measure these stresses. [4,5].

In this research, the non-pillar continuous exploitation method and Miami mining method were used. There are, of course, other methods as well, such as design methods and stability analyses involving empirical methods, observational methods, analytical methods, and numerical methods [6,7]. Numerical methods can be used for the analysis of the excavation stages, pillar, and stope dimensions [8]. Also, it is possible to use them for defining plastic zones around underground openings [9]. The pillars should be strong enough to tolerate the overburdened stress. Chehel Koureh mine is located 110 km NW of Zahedan city in Iran. Chehel Koureh mine belongs to the Eocene age and consists of two units, Ef1 (alternating shale and sandstone) and Ef2 (sandstone). To date, different researchers have investigated the pillar stability of underground openings and pillars' recovery safety, and have recommended different methods [10-12].

2. Structural geology of ore body

The principal joint sets were achieved to analyze fractures of the area. For this reason, the joints were projected on stereonet and four principal joints were identified in the area. The dip and dip directions of these joints are presented in Table 1 [10].

3. RMR results

As shown in Table 2, RMR for this rock mass is calculated 53 which is classified as fair rock.

* Corresponding author. Tel: +98-3133915115, Fax: +98-3133912776, *E-mail address:* cheraghi@cc.iut.ac.ir (M. Cheraghi Seifabad).

Table 1. Joint sets at the studied area

No.	Joint sets	Dip (°)	Strike (°)
1	J_1	67 NW	N69 E
2	J_2	66 SW	N43 W
3	J_3	62 NE	S28 E
4	J_4	29 NW	N3 E

Table 2. RMR results at the studied area

Parameter	Rating
Uniaxial Compressive Strength	R1=7
RQD	R2=8
Spacing of joints	R3=10
Joint conditions	R4=13
Water conditions	R5=15
	RMR=53

4. Geological Strength Index (GSI) results

Geological Strength Index is used for surface and underground structures. It was introduced by Hoek et al. in 1997[13]. Then, Sonmez and Ulusay (1999) added modifications to it and ultimately in 2002, Hoek et al. implemented the last modifications [14].

To quantify the mentioned classification, structural rating (SR) has been used in the vertical axis as shown in Figure 1. SR depends on the number of joints in each cubic meter (J_v). GSI graph is a general description of discontinuities surface conditions and can be specified with (SR). This rating is based on joint roughness (R_r) value, weathering intensity (R_w), type of infilling, and joint spacing value (R_f), divided into 5 sections. The parameters R_r, R_w, and R_f can be obtained using Table 3.

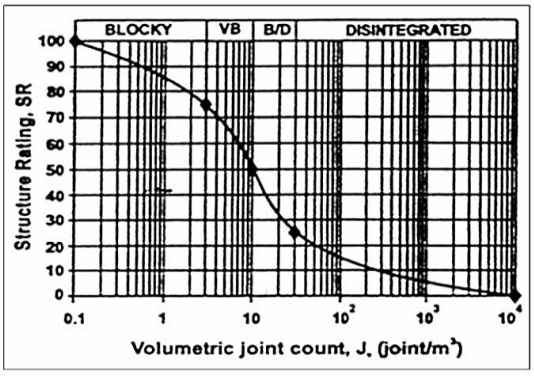

Figure 1. The relationship between SR and J_v

GSI is defined with SR and SCR values. The strength parameters of rock mass are achieved using available relations. Based on Hoek s' recommendation, the GSI value is described as a range of values. Therefore, the GSI value is obtained as 38. Also, GSI is calculated through Equation 1. using RMR as follows:

$$GSI=RMR_{89}-5 \quad (1)$$

Thus, the GSI value is calculated as 48 using the above equation and it can be said that the GSI value varies in the range of 38-48. The range of geomechanical parameters related to intact rock and rock mass is defined through lab and in situ tests in the Chehel Koureh mine. Considering rock mass classification of the stope site and the available empirical relations, the geomechanical parameters are defined. There are conventional methods to define the compressive strength of rock mass such as empirical failure criteria, empirical rules, back analysis, large scale tests, and mathematical modeling. Different researchers have presented different empirical rules based on rock mass classification to define the compressive strength of rocks. Table 4 shows different compressive strength indexes for Chehel Koureh mine.

5. Rock mass deformation modulus

The empirical relations are utilized to estimate rock mass deformation modulus presented by different researchers (Table 5).

6. Internal friction angle and cohesion of rock mass

Internal frictional angle and cohesion of rock mass are defined according to GSI and RMR classifications for the studied area (Tables 6-8).

7. In situ stresses

Brady and Hoek presented the vertical stresses based on empirical results. Also, Arjang has reported the material stresses based on empirical data from Canada. He considered an average weight of 0.026 MPa/m for most rocks (Table 9).

8. Numerical methods

Empirical methods are not the only way to solve the complex issues of underground excavation. Thus, most specialists have recommended both numerical and empirical methods to find accurate results. In this research, as the rock mass is of fair quality based on GSI and RMR classifications, the rock mass is considered as an equivalent continuum and is thus modeled with FLAC 3D software [31].

9. FLAC 3D software

FLAC 3D is based on Lagrangian calculations, which is suitable for large deformations. This software has different behavioral models, which allows simulating models with different linear and non-linear behaviors of materials.

10. Modeling of stope in non-pillar exploitation method

In the non-pillar exploitation method, after excavation of two horizontal tunnels being apart in height of 40 m, the excavation of stope was carried out according to Figure 2. Each stope was divided into two sub-stopes, A and B. Sub-stope A was excavated in the longitudinal direction with 15 m length. Sub-stope B was 35 m in length. A support wall of the ore body was left between sub-stopes A and B. First, the ore material of sub-stope A was excavated. Then, it was filled with cement and waste materials, subsequently, the excavation of sub-stope B was started. To create free space for movement of drilling machine freely above sub-stopes A and B, a cylindrical pillar was left above the support wall to provide safety for the drilling machine. The dimensions of this pillar play an important role in the roof stability of the drilling machine space. Too large a dimension is an obstacle for drilling machines, and too small causes instability [32].

As seen in the above-mentioned Figure, B-B is the longitudinal section at the direction of the ore body, A-A is a transversal section from the horizontal view, and C-C is a transversal section from the vertical view. In this research, as shown in Figure 3, a geometrical model is created based on FLAC3D software with the dimension 300 m length, 300 m height, and 160 m width. As the exploitation stope has 55 m length, 20 m width, and 40 m height, it is better to consider the distance of boundary to exploitation stope 8 times half the width of the stope from each side. The exploitation stope is located in the center of the model. The different colors related to stope show the excavation stages, specified with numbers. The support wall is presented above the stope. In the non-pillar exploitation method, after excavation of the fourth stage, the early spaces are fitted with cement and waste materials (5^{th} stage). Also, after the completion of the 7^{th} stage excavation, all the empty spaces of the stope and drilling machine room are filled.

Table 3. The values of parameters R_r, R_w, and R_f in GSI classification

Roughness rating	Very rough	Rough	Slightly rough	Smooth	Slickensided
Rating (R_r)	6	5	3	1	0
Weathering	None	Slightly weathering	Moderately weathering	Highly weathering	Decomposed
Rating (R_w)	6	5	3	1	0
Infilling	None	Hard (<5 mm)	Hard (>5 mm)	Soft (<5 mm)	Soft (>5 mm)
Rating (R_f)	6	4	2	2	0
SCR=R_r+ R_w+ R_f					

Table 4. Empirical formulas for defining compressive strength of rock mass [15- 22]

	Equation	Calculated value
Hoek and Brown(1980)	$\sigma_{Cmass} = \sigma_{Ci}\sqrt{e^{(\frac{RMR-100}{9})}}(MPa)$	4.71
Yudhbir et. al. (1983)	$\sigma_{Cmass} = \sigma_{Ci}e^{(7.65(\frac{RMR-100}{100}))}(MPa)$	1.76
Ramamurthy (1986)	$\sigma_{Cmass} = \sigma_{Ci}\, e^{(\frac{RMR-100}{18.75})}\quad (MPa)$	5.23
Kalamaris and Bieniawski (1995)	$\sigma_{Cmass} = \sigma_{Ci}\, e^{(\frac{RMR-100}{24})}\quad (MPa)$	9.04
Sheorey (1997)	$\sigma_{Cmass} = \sigma_{Ci}\, e^{(\frac{RMR-100}{20})}\quad (MPa)$	6.11
Trueman (1998)	$\sigma_{Cmass} = 0.5\, e^{(0.06RMR)}\quad (MPa)$	12.02
Aydan and Dalgic (1998)	$\sigma_{Cmass} = \left(\frac{RMR}{RMR+\beta(100-RMR)}\right)\sigma_{Ci}(MPa), \beta = 6$	10.14
Hoek (2002)	$\sigma_{Cmass} = \left(\frac{\sigma_{Ci}(m_b+4s-a(m_b-8s))(\frac{m_b}{4}+s)^{a-1}}{2(1+a)(2+a)}\right)(MPa)$	8.59

σ_{ci} (64.11) is UCS of intact rock (MPa)
a =0.509, s=0.0018, mb=1.45 Constants
E_i (24.46×10^3) is the elasticity of rock mass (in MPa)
γ (2.5) density of rock mass (t/m³)

Table 5. Empirical equation of different researchers to define rock mass modulus [23- 30]

	Equation	Calculated value
Bieniawski (1978)	$E_{mass} = 2RMR - 100(GPa)$, RMR > 50	6
Verman (1993)	$E_{mass} = 0.3H^{\alpha}10^{(\frac{RMR_{1979}-20}{38})}(GPa), H > 50m$	11.4
Mitri (1994)	$E_{mass} = E_i\left[0.5\left\{1-\left(\cos\pi\times\frac{RMR}{100}\right)\right\}\right](GPa)$	18.71
Hoek and Brown (1997)	$E_{mass} = \sqrt{\frac{\sigma_{Ci}}{100}}\times 10^{(\frac{GSI-10}{40})}(GPa), \sigma_{Ci} < 100MPa$	5.35
Read et al (1999)	$E_{mass} = 0.1\left(\frac{RMR}{10}\right)^3(GPa)$	14.89
Ramamurthy (2001)	$E_{mass} = \left(\frac{E_i\, exp(\,RMR-100)}{17.4}\right)(GPa)$	5.44
Hoek (2002)	$E_{mass} = \left(1-\frac{D}{2}\right)\times\sqrt{\frac{\sigma_{Ci}}{100}}\times 10^{(\frac{GSI-10}{40})}(GPa)$	3.21
Ramamurthy (2004)	$E_{mass} = E_i e^{(-0.0035\times.003500-RMR)))}(GPa)$	10.75
Hoek and Diederichs (2006)	$E_{mass} = E_i\left(0.02+\frac{1}{1+e^{(\frac{60+15D-GSI}{11})}}\right)(GPa)$	2.12

σ_{ci} (64.11) is UCS of intact rock (MPa)
E_i (24.46×10^3)is the elasticity modulus of rock mas (in MPa)
D=0.8 (Disturbance factor)
α: For strong rocks (0.16) and weak rocks (0.35)

Table 6. Values and classification of rock mass strength parameters based on RMR

Rating	81-100	61-80	41-60	21-40	Less than 20
Rock mass class	I	II	III	IV	V
Description	Very good rock	Good rock	Fair rock	Poor rock	Very poor rock
Cohesion (kPa)	More than 400	300-400	200-300	100-200	Less than 100
Internal friction angle (Degrees)	More than 45	35-45	25-35	15-25	Less than 15

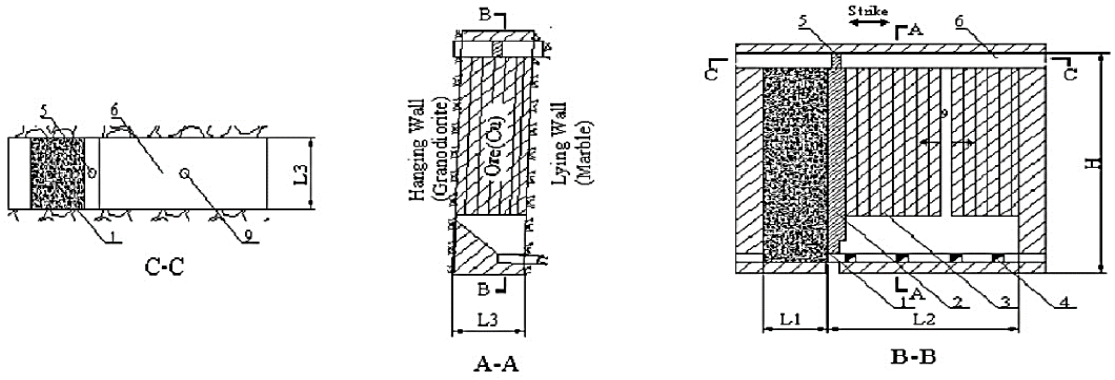

Figure 2. The exploitation stope in three conditions [32]

Figure 2. Shows numbers and symbols as follows:
1-Sub-Stope A 2-Supported wall between two stopes
3-Sub-Stope B 4-Below the stope (Transport tunnels below the cones) 5-The pillar of the ore body 6-Drilling room (location of drilling machine)
7 and 8-Horizontal transport tunnels and vertical shaft, respectively
9-Blastholes L_1-Length of sub-stope A L_2 –Length of sub-stope B L_3-Width of the ore body (Width of stope) H-Height of the stope

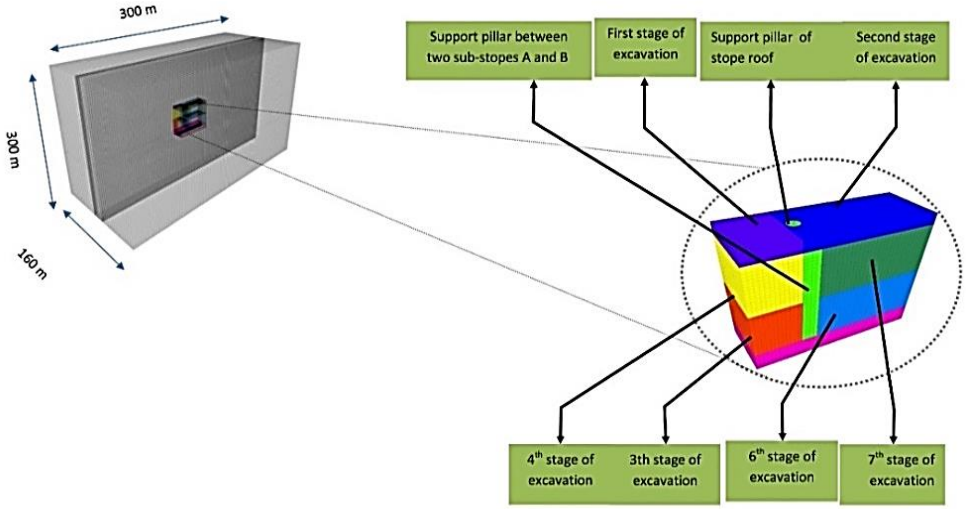

Figure 3. Geometrical model using FLAC3D software and sequence of excavations

Table 7. Shear strength parameters based on RMR for the studied area

Type of rock	Cohesion (kPa)	Class	RMR	Internal friction angle (Degrees)
Fair rock	200-300	III	53	25-35

Table 8. Geomechechnical parameters of rock mass in the studied area using Rocklab software

Type of rock	σ_{ci} (MPa)	GSI	Rock mass parameters			
			$C(kPa)$	$\phi(°)$	$\sigma_{cm}(MPa)$	$E_m(GPa)$
Fair rock	64.11	38-48	629	46.24	8.515	5.18

Table 9. in situ stress definition

	Equation	Calculated value
Brady and Hoek (1978)	$\sigma_v = 0.027H(MPa)$	3.24
Arjang (1998)	$\sigma_v = 0.026H(MPa)$	3.12

11. Behavioral model selection

There are different behavioral models in FLAC3D software which can be utilized according to the conditions of the problem. Due to the compatibility of the Hoek-Brown behavioral model with rock mass

behavior, this behavioral model was used to analyze the support wall above the stope. Also, this model can be used to specify the parameters related to the plasticity such as the degree of the damage induced during construction. The required parameters, obtained based on empirical equations and different tests, for using the mentioned behavioral model to analyze the rock mass stope are summarized in Table 10.

Table 10. The required parameters for the Hoek-Brown model at the studied area

Parameter	Value
UCS of intact rock (MPa)	64.11
UCS of rock mass (MPa)	8.59
Geological Strength Index (GSI)	43
Elasticity modulus of intact rock (MPa)	24460
Elasticity modulus of rock mas (MPa)	5.11
Cohesion (kPa)	200
Poisson's ratio	0.2
Internal friction angle (Degrees)	40
Density of rock mass (kN/m³)	25
Hoek-Brown constant for intact rock (m_i)	8
Hoek-Brown constant for rock mass (m_b)	1.044
Disturbance factor (D)	0
Rock mass constant (s)	0.509
Rock mass constant (a)	0.002

12. Excavation stages and filling of the stope

12.1. First stage of excavation

As shown in Figure 4, in this stage, the upper part of stope in the left pillar is removed and the model is solved.

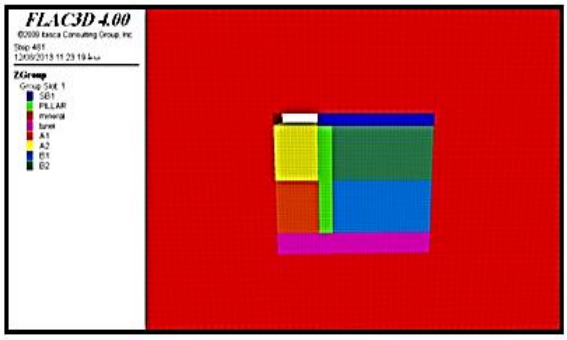

Figure 4. The first stage of excavation of stope

12.2. The second stage to 5th stage of excavation

In the second stage, the upper part in the right pillar is removed. In the third stage, the lower part of sub-stope A is removed. The excavation stages are shown in Figures 5-7.

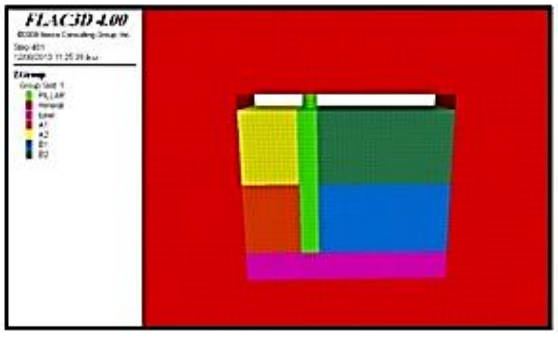

Figure 5. The second stage of excavation of stope

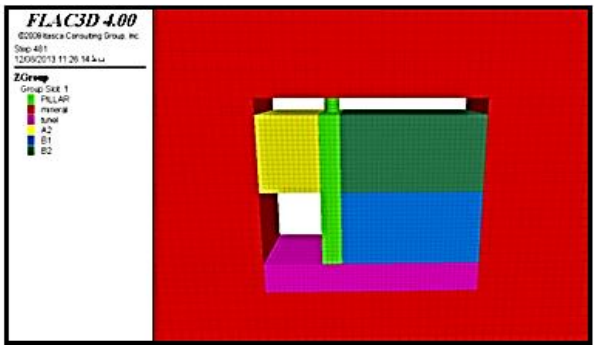

Figure 6. The third stage of excavation of stope

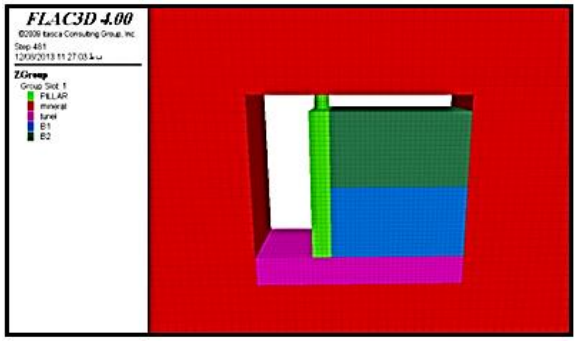

Figure 7. The fourth stage of excavation of stope

12.3. Fifth stage (Filling of empty spaces in excavation stages of 3 &4)

This part is shown in Figure 8. In this stage, the upper and lower part of sub-stop A removed before is filled with cement and waste materials. Then, for these materials, the Mohr-Coulomb is chosen to solve the model. The geomechanical characteristics of these filling materials are presented in Table 11.

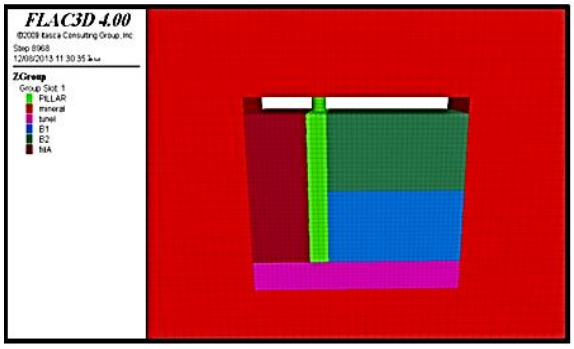

Figure 8. The fifth stage of excavation of stope

Table 11. Geomechanical parameters of filling materials for Mohr-Coulomb criterion

Parameter	Filling material properties
UCS of intact rock (MPa)	3.5
Tensile strength (MPa)	0.5
Young's modulus (MPa)	1000
Poisson 'ratio	0.3
Cohesion (MPa)	0.65
Internal friction angle (Degrees)	35
Density of rock mass (KN/m³)	22.1

12.4. 6th to 7th stages of excavation

In this part, at first, the lower section of sub-stope B and then the upper section of sub-stope B are removed. The excavation stages are shown in Figures 9, 10.

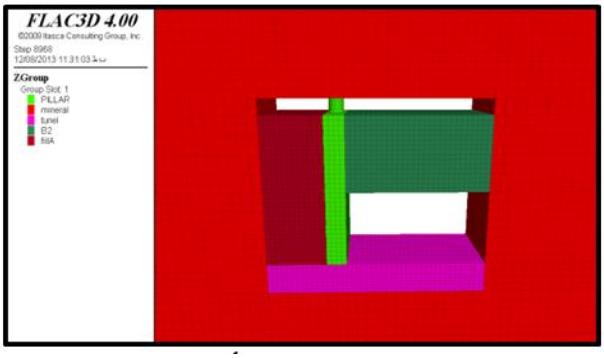

Fig 9. The 6th stage of excavation of stope

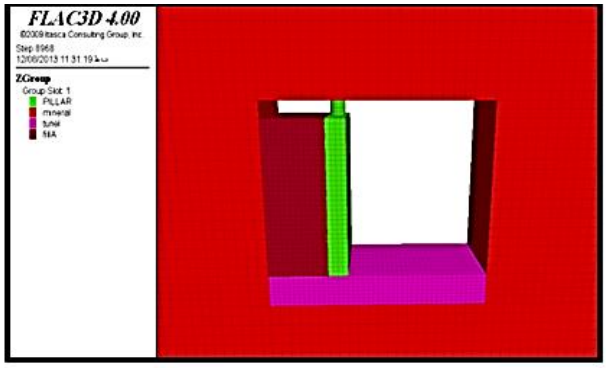

Figure 10. The 7th stage of excavation of stope

12.5. The 8th stage of excavation

This part is shown in Figure 11. In this stage, the upper and lower sections of sub-stope B removed before are filled with cement and waste materials. Then, the Mohr-Coulomb criterion is chosen to solve the model. The geomechanical characteristics of the filling materials were provided above.

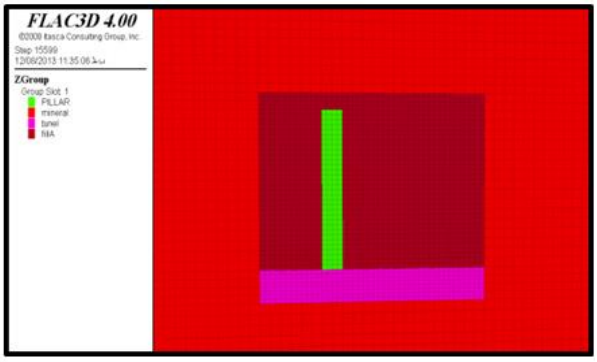

Figure 11. The last stage of excavation as filling the empty spaces

13. The selection of critical stages in pillar stability

The maximum displacement of the roof and ground surface, and the creation of a plastic zone around the pillar occur in the 7th stage when emptiest spaces are created in the stope. This is shown in Figure 12.

14. Analysis of pillar dimensions

After 7th stage of excavation, because of the emptiest spaces in the stope, we face the most critical stage for the stability conditions of the pillar. As mentioned before, the height of this pillar is always constant (3.8 m) relative to the height of the drilling machine. Thus, the diameter of the pillar is chosen to analyze the pillar dimensions. It is necessary to mention that the oversize diameter of the pillar reduces the maneuverability power of the drilling machine. For the selection of desirable diameter in the pillar, at first 5 different diameters (3, 3.2, 3.4, 3.6, 3.8) are considered and then two methods are utilized for the analysis. The first method concerns subsidence conditions in the ground surface specified by measuring the critical surface (or height). The second method is the creation of the plastic zone around the pillar.

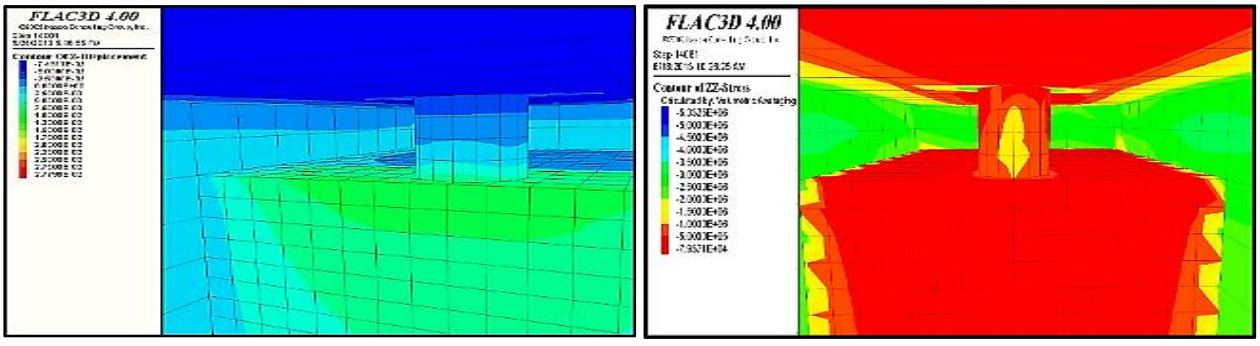

Figure 12. The excavation stage at exploitation stope excavated model, displacement contours at the pillar and its surrounding (left), and vertical stress contours around the pillar (right).

15. Analysis of the pillar diameter using subsidence parameters

The subsidence conditions for each pillar diameter and draw area in the ground surface are specified with FLAC software and then, the horizontal distance of draw area relative to the edge of stope in left and right sides at the ground surface is defined. Also, the angle of the draw for each side is calculated and finally, the critical height of each pillar diameter is defined. As shown in Table 12, the supercritical height is created if the pillar diameter is equal to 3 m or less. To determine the suitability of the other four-pillar diameters (3.2, 3.4, 3.6, 3.8), the analysis of pillar diameter is implemented by the assessment of the plastic zone around the pillar

16. Pillar diameter analysis using assessment of plastic zone

The plastic zone or peeling around the pillars and galleries is called the damage zone [22]. The four-pillar diameters which were suitable before,

due to lack of subsidence at the surface, are investigated according to the plastic zone around the pillar. The lack of a plastic zone represents the stability of the pillar. Then, the suitable diameter will be specified for the stability of the pillar and the stope.

Table 12. The results obtained from pillar diameters according to a critical height

Pillar diameter (m)	3	3.2	3.4	3.6	3.8
The distance from center of the excavation at right side (m)	23.8	31	46	54	85.1
The distance from center of the excavation at left side (m)	29	39.6	58	89.6	102.3
Angle of draw (Right-degrees)	16.6	21.14	30	34	46.8
Angle of draw (Left-degrees)	20	26.33	36	48.2	52
Critical height (m)	83.5	62.4	42.4	30.7	23.5

17. Plastic zone around the pillar in the 7th stage of excavation

The plastic zone is created around the pillar as shown in Figures 13, 14, 15, and 16. The positive contours of stresses around the pillar reaffirm this condition. (Around the pillar, red color shows: +128 kPa stress for diameter 3.2; +112 kPa for diameter 3.4, +104 kPa for diameter 3.6). Therefore, these pillar diameters are not suitable for the support of the stope roof [11,12,33]. Figure 16. shows that the plastic zone is not created around the pillar and the stope roof. Negative contours of stress with the least value, i.e., -79.4 (Red color), indicate that the pillar with a 3.8 m diameter is suitable for the support of the stope roof.

18. Safety factor definition for the pillar of 3.8 m diameter

The method of strength reduction is utilized to calculate safety factors using FLAC3D software. Using this method for the stability analysis, different C and φ values (Cohesion and internal friction angle) are considered as the test conditions. The highest values of these two parameters are the natural values, at which the model gets balanced.

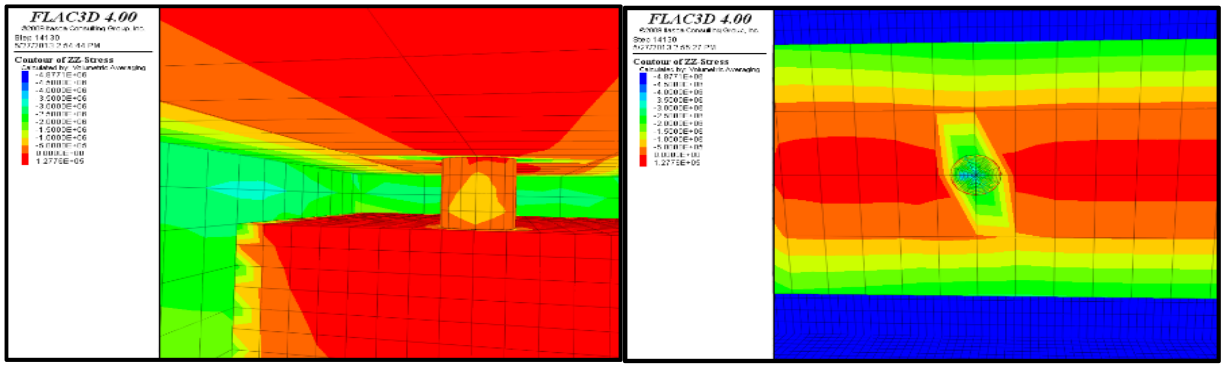

Figure 13. Stress contours around the pillar of 3.2 m diameter

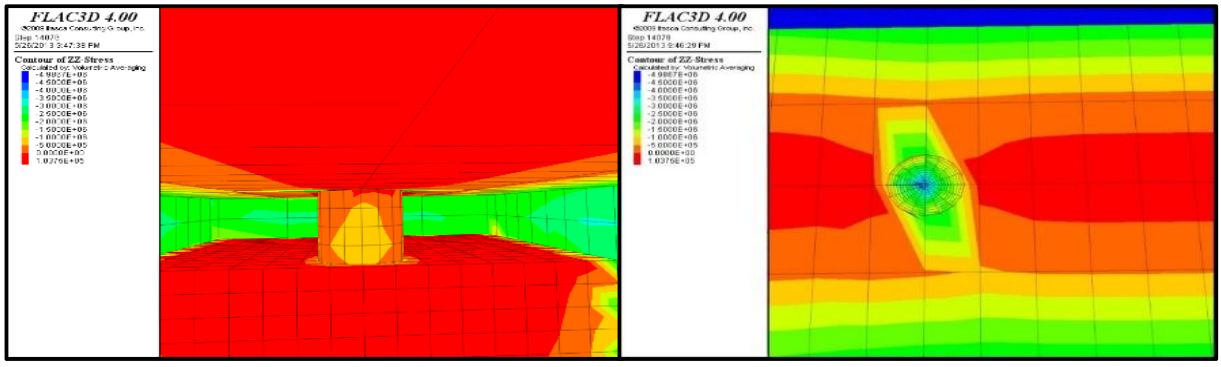

Figure 14. Stress contours around the pillar of 3.4 m diameter

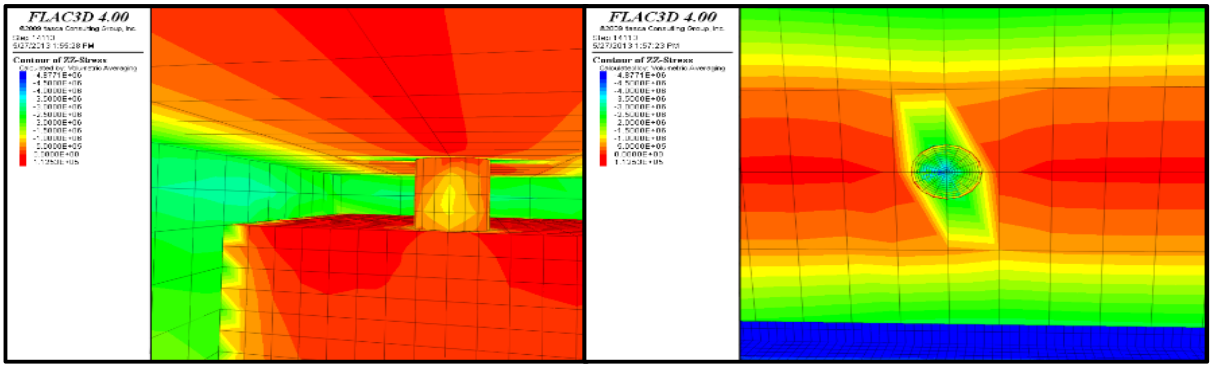

Figure 15. Stress contours around the pillar of 3.6 m diameter

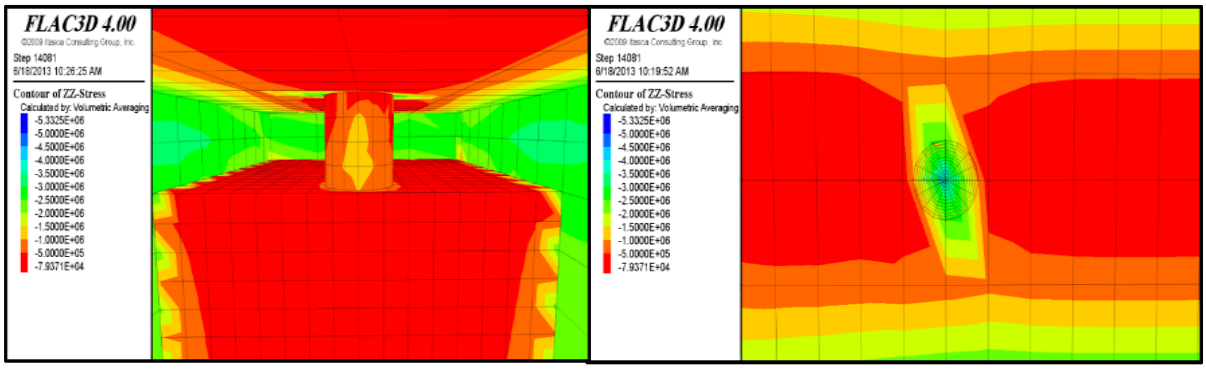

Figure 16. Stress contours around the pillar of 3.8 m diameter

Finally, equation (3) is used for the calculation of the pillar safety factor. In this equation, C and φ are cohesion and internal friction angle, respectively, in pillar stability conditions. Generally, this equation represents the relationship between stable and unstable conditions. There are many different standards in the literature for stability analysis (Figure 17).

$$C^{'}=\left(\frac{1}{SF}\right)\times C \quad (2)$$

$$SF=\frac{\tan\varphi available}{\tan\varphi required} \quad (3)$$

Where C' and $\varphi_{required}$ are cohesion and internal friction angle, respectively, at the last stage of analysis (The stage which creates tension zone around the pillars). As C and φ values are 200 kPa and 40 degrees, respectively, in natural conditions of the rock mass around the stope, the model is balanced by considering the Mohr-Coulomb criterion at the 7th stage of excavation with 3.8 m diameter pillar. Then, C and φ are reduced according to equations (2) and (3), and the model is solved again. If the tension area around the pillar is created, the calculation is not continued. Otherwise, the trend of lowering those two parameters is continued until the tension area is created around the pillar.

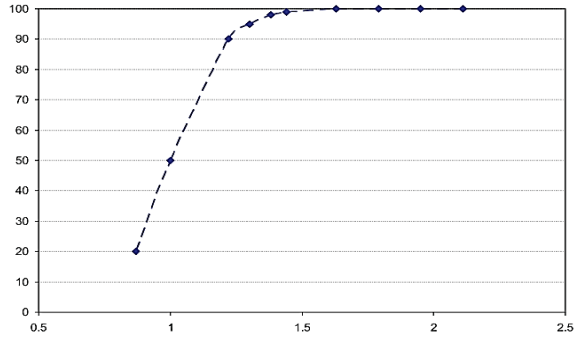

Figure 17. Stability probability of underground structures [34].

Finally, in the last stage where tension area is created, C and φ are plugged into Equation (4) instead of C' and $\varphi_{required}$ respectively. In this way, the safety factor is determined. The stress conditions at a point in the pillar are shown in Figures 18, 19, 20, according to different cohesion and internal friction angles. In Figures 18 and 19, the stress values are in negative areas indicating a lack of tension areas. In Figure 20, as shown, the stress value includes a positive area which represents the tension area around the pillar. Thus, by considering the cohesion and friction angle in Equation (4), the safety factor is calculated as follows:

$$SF=\frac{\tan 40}{\tan 37}=1.11 \quad (4)$$

There is a need for a special drilling machine which can operate at the limited height and width of the stope. Also, the machine should be able to drill holes of 40 m depth. Below the stope, a vibration machine is needed to help transfer the excavated materials to transport tunnels. Since the technology required is not available in Iran, the Miami exploitation method is selected. Through the combined method, which is called shrinkage and pillar caving or the Miami method, the ore body is excavated with the pillars left between them. After completion of the shrinkage method, the supporting pillars of the stope roof are destroyed and recovered. In Figure 21, the cross-section of the stope (right side) is shown and the pillar conditions are presented.

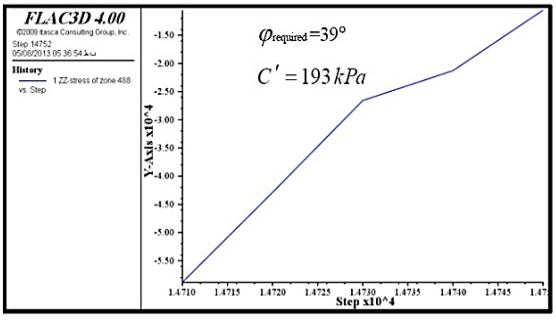

Figure 18. Stress condition at a point around the pillar with a friction angle of 39 Degrees

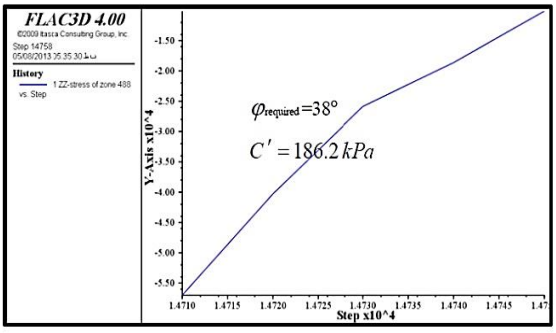

Figure 19. Stress condition at a point around the pillar with a friction angle of 38 degrees

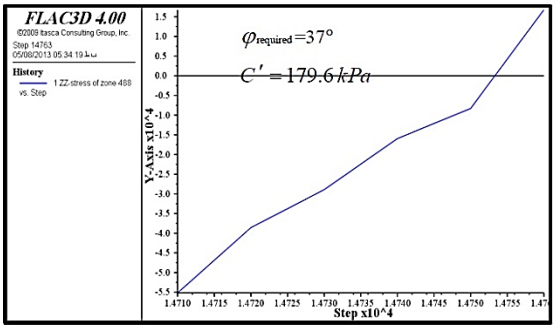

Figure 20. Stress condition at a point around the pillar with a friction angle of 37 degrees The Miami exploitation method for Chehel Koureh mine

19. Geometrical model for Miami exploitation method using FLAC3D

The model is created by FLAC3D software in the dimensions of 240 m length, 200 m height, and 160 m width (Figure 21).

To ensure that the model is balanced, the history of unbalanced forces needs to be investigated. Also, Figure 22 shows vertical stresses contours in natural ground conditions.

20. Pillar stability analysis using assessment of plastic zone

As there are three stopes and two supporting pillars in this method, the most critical condition arising from strength and pillar stability occurs when one of the pillars is destroyed. The analysis of the remaining pillar is carried out at this critical stage.

At this point, the plastic zone around the supporting pillar in different widths of the pillar is investigated (Figures 23, 24, and 25)

According to stress contours around the pillars for three different widths (5, 6, 8 m), the plastic zone is not created around the pillar when the pillar width is 8 m. Figure 26 shows the stress conditions of a zone in the pillar (Red circle in Figure 26).

Because the vertical and horizontal stresses are negative, which indicates the stability of the pillar, the 8 m width is suitable for this pillar.

21. Safety factor definition for the pillar of 8 m width

The stress conditions at a point in the pillar are shown in Figures 27, 28, 29, 30, and 31. As shown in Fig 32, the stress value reaches the positive area, and the tension area begins. Thus, by substituting cohesion and internal friction angle into Equation (2), the stability factor is calculated as follows (Equation 5):

$$SF=\frac{\tan 40}{\tan 28}=1.58 \quad (5)$$

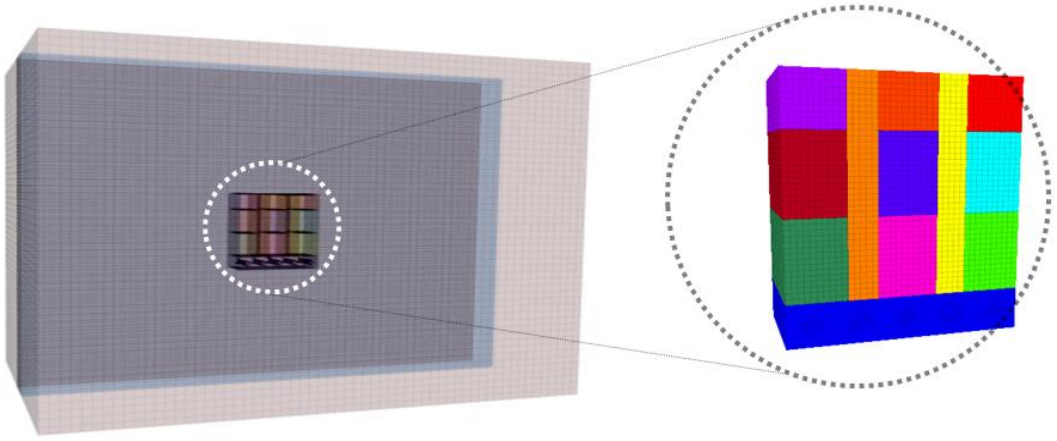

Figure. 21. Geometrical model for Miami method using FLAC3D

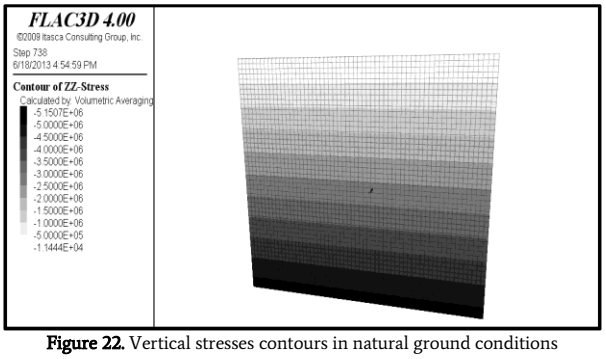

Figure 22. Vertical stresses contours in natural ground conditions

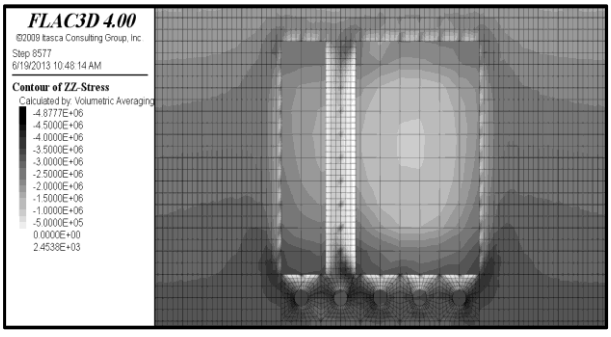

Figure 24. Stresses contours with the remaining pillar of 6 m width

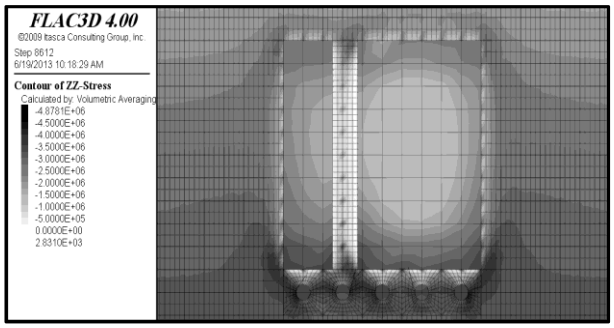

Figure 23. Stresses contours with the remaining pillar of 5 m width

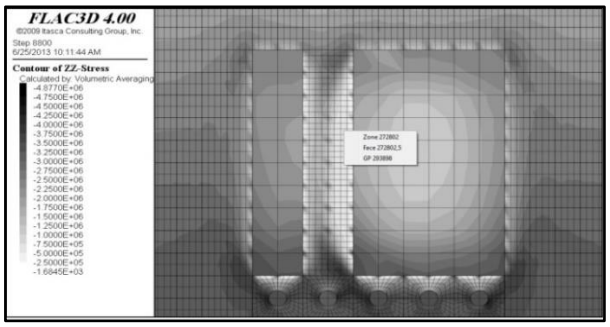

Figure 25. Stresses contours with the remaining pillar of 8 m width

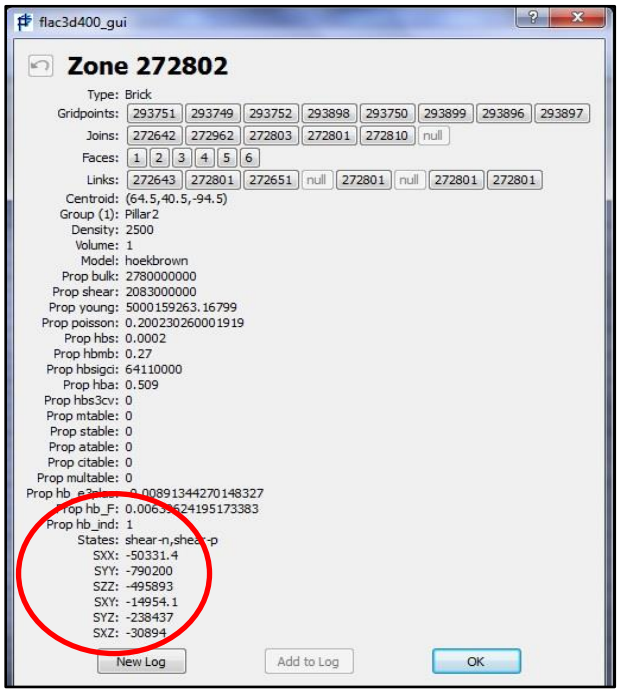

Figure 26. Geometrical characteristics of a selected zone in the pillar (Pillar diameter: 8 m)

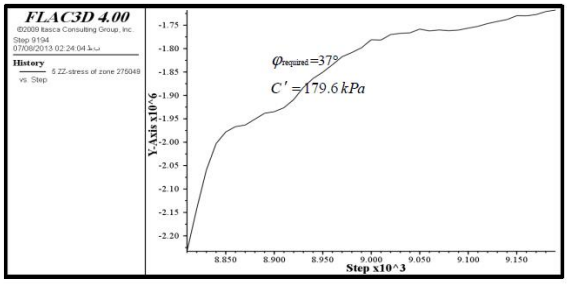

Figure 27. Stress condition at a point around the pillar with an internal friction angle of 37 degrees

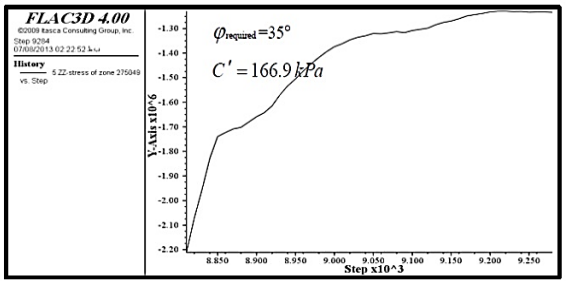

Fig 28. Stress condition at a point around the pillar with an internal friction angle of 35 degrees

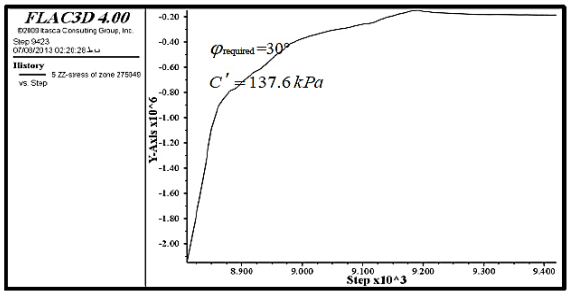

Figure 29. Stress condition at a point around the pillar with an internal friction angle of 30 degrees

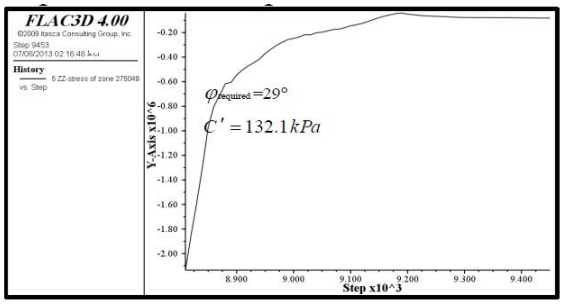

Figure 30. Stress condition at a point around the pillar with an internal friction angle of 29 degrees

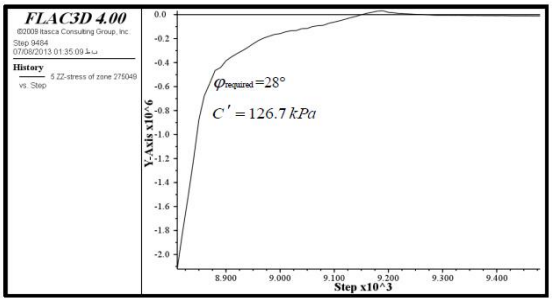

Figure 31. Stress condition at a point around the pillar with an internal friction angle of 28 degrees

22. Conclusions

1) Considering the strength characteristics of rock mass and thickness of ore body, non-pillar and Miami method was selected as the suitable method for exploitation of Chehel Koureh mine. The non-pillar method compared with the Miami method has a high ability of mechanization, and is thus more effective with respect to the speed of operation and efficiency. Generally, this method compared to the Miami method is less expensive since it reduces the operation time.

2) In the non-pillar method, the pillar with a 3.8 m diameter was regarded as suitable to support the roof of the drilling machine. The safety factor was calculated at 1.11, which is nearly fair for pillar safety. In the Miami exploitation method, the pillar of 8 m width was suitable for the support of the stope roof. The safety factor was obtained at 1.58, which is fair in terms of the safety factor.

3) Because of limitations in non-pillar methods, such as the type of drilling machine and special vibration apparatus, the Miami method was selected as an applicable method for the exploitation of the Chehel Koureh mine.

References

[1] Tesarik, D.R., Seymour, J.B., &Yanske, T.R. (2003). Post-failure behavior of two mine pillars confined with backfill , International Journal of Rock Mechanics & Mining Sciences., 40 (0), 221–232.

[2] Bogert, H.,Jung, S.J., & Lim, H.W. (1997). Room and pillar stope design in highly fractured area, International Journal of Rock Mechanics & Mining Sciences., 34 (0), 145-159.

[3] Li, Z., Liu, H., Dai, R., & Su, X. (2005). Application of numerical analysis principles and key technology for high fidelity simulations to 3-D physical model tests for underground caverns, Tunneling and underground space Technology., 20 (0), 390-395.

[4] Hammett, R.D., Hoek, E. (1981). Design of large underground caverns for hydroelectric projects with particular reference to structurally controlled failure mechanisms. ASCE Spring

Convention, New York Session on Rock Mechanics of Large Hydro Projects.

[5] Martin, C.D ., Kaiser, P.K., & Christiansson, R. (2003). Stress, instability and design of underground excavations., International Journal of Rock Mechanics & Mining Sciences., 40 (0), 1027-1047.

[6] Stille, H., Palmstrom, A. (2003). Classification as a tool in rock engineering", Tunneling and Underground Space Technology., 18, 331-345.

[7] Hudson, J.A. Feng, X.T. (2007). Updated flowcharts for rock mechanics modelling and rock engineering design, International Journal of Rock Mechanics & Mining Sciences., 44 (0), 174-195.

[8] Jing ,L.,Hudson, J.A. (2002). Numerical methods in rock mechanics, International Journal of Rock Mechanics & Mining Sciences, 39 (0), 409-427.

[9] Palassi, M., Asadollahi, P. (2012). Development of plastic zone around underground excavations, University of Tehran.

[10] Kavoshgaran Consulting Engineering Company. (1996). Chehel Koureh mine design.

[11] Ghasemi, E., Shahriar,K., & Sharifzadeh,M. (2012). A new method for risk assessment of pillar recovery operation, Safety Science., 50 (0), 579–585.

[12] Wang, S. Y., Sloan, S. W., Huang, M. L., & Tang, C. A. (2011). Numerical Study of Failure Mechanism of Serial and Parallel Rock Pillars, Rock Mech Rock Eng., 44 (0), 179–198.

[13] Hoek, E. Brown, E.T (1997). Practical estimates of rock mass strength. Int. J. Rock Mech Min Scin, 34(8), 1165-86.

[14] Sonmez, H., Ulusay, R. (1999). Modifications to the geological strength index (GSI) and their applicability to rock slopes. Int. J. Rock Mech Min Scin, 36(8), 743-760.

[15] Hoek, E. Brown, E.T. (1980). Underground excavations in rock. Inst. Min Metall, Lonodon, Uk.

[16] Yudhbir, A., Lemanza, W., & Prinzl F. (1983). An empirical failure criterion for rock masses. In: Proceedings of the fifth international congress on rock mechanics, Melbourne, Australia.

[17] Ramamurthy, T. A. (1986). Stability of rock mass. 8 th Annual lecture. Indian Geotech. J. 1-74.

[18] Kalamaris, G. S., Bieniawski, Z. T. (1995). A rock mass strength concept for coal incorporating the effect of time, Proceedings of the eight international congress on rock mechanics, Rotterdam: Balkema.

[19] Shoerey, P.R. (1997). Empirical rock failure criteria, Rotterdam : Balkema.

[20] Trueman R. (1988). An evaluation of strata support techniques in dual life gate roads. PhD Thesis. Univ Wales, Cardiff. Uk.

[21] Aydan, O. Dalgic, S. (1998). Prediction of deformation behavior of 3 lanes Bolu Tunnel through squeezing rocks of North American Fault Zone (NAFZ), Proceedings of the regional symposium on sedimentary rock engineering, Taipei, Taiwan.

[22] Hoek, E. Carranza-Torres, C.T., & Corkum, B. (2002). Hoek-Brown failure criterion-2002 edition. Proceedings of the 5th North American Rock Mechanics Symposium, Toronto, Canada.

[23] Bieniawski, Z.T. (1978). Determining rock mass deformability: experience from case histories," Int. J. Rock Mech Min Scin Geomech Abstr. 15 (0), 237-247.

[24] Verman, M.K. (2018). Rock Mass-Tunnel Support Interaction Analysis. Available online: http://shodhbhagirathi.iitr.ac.in:8081/xmlui/handle/123456789/1322.

[25] Mitri, H., Edrissi, R., & Henning, J. (1994). Finite-element modeling of cable-bolted stopes in hard-rock underground mines, " at SME annual meeting, New Mexico, Albuqueurque, USA.

[26] Hoek, E., Brown, E.T. (1997). Practical estimates of rock mass strength. Int. J. Rock Mech Min Scin, 34(8), 1165-86.

[27] Read, S. A. L., Richards, L. R., & Perrin, N. D. (1999). Applicability of the Hoek-Brown failure criterion to New Zealand greywacke rocks, Proceedings 9th International Society for Rock Mechanics Congress, Paris, France.

[28] Ramamurthy, T. A. (2001). Shear strength response of some geological materials in triaxial compression, Int J Rock Mech Min Sci 2001, 38 (0), 683-97.

[29] Ramamurthy, T. A. (2004). Geo-engineering classification for rocks and rock masses, Int J Rock Mech Min Sci 41 (0), 89-101.

[30] Hoek, E., Diederichs, M. S. (2004). Empirical estimation of rock mass modulus, Int. J. Rock Mech Min Scin, 43(2), 203-215.

[31] Itasca Consulting Group. (2009). FLAC3D, Fast Lagrangian Analysis of Continua in 3 Dimensions, version 4, User's Manual.

[32] Deng, J., Yue, Z.Q., Tham, L.G., & Zhu, H.H. (2003). Pillar design by combining finite element methods, neural networks and reliability: a case study of the Feng Huangshan copper mine, China,International, Journal of Rock Mechanics & Mining Sciences., 40 (0), 585–599.

[33] Esterhuizen, G.S., Dolinar, D.R., & Ellenberger, J.L. (2011). Pillar strength in underground stone mines in the United States, International Journal of Rock Mechanics & Mining Sciences., 48 (0), 42–50.

[34] Hill, D. (2005). Coal Pillar Design Criteria for Surface Protection, Coal Operators, Conference, University of Wollongong & the Australasian Institute of Mining and Metallurgy., Austarlia

[35] Hill, D. (2005). Coal Pillar Design Criteria for Surface Protection, Coal Operators, Conference, University of Wollongong & the Australasian Institute of Mining and Metallurgy., Austarlia.